Chapter 7
FOC Error Sources

In This Chapter...

The pipeline processing described in the previous chapter attempts to remove most of the instrumental signatures of the FOC detector. Pipeline processing does not remove all of the instrumental features because some of the FOC's properties are either time dependent, varying in a random way that precludes correction, or else difficult to correct without introducing other errors. This section highlights some limitations of the pipeline calibration and certain other effects that the pipeline does not address.

7.1 Overview of FOC Characteristics

Table 7.1 lists certain effects owing to the design of the FOC detector, optics, and electronics that afflict all FOC images and indicates whether the pipeline corrects for them. .

The diagram below (Figure 7.1) describes where these various instrumental characteristics arise.

Table 7.1: Characteristics Corrected in Standard Pipeline

Characteristic	Pipeline Corrected?
Nonlinearity and saturation	No
Geometric distortion	Yes
Flatfield residuals (i.e., blemishes, reseau marks, defects, and video effects)	No
Format-dependent sensitivity	Yes
Background noise	No
Filter-induced image shifts	No
Point spread function	No

Figure 7.1: Sources of Instrumental Characteristics

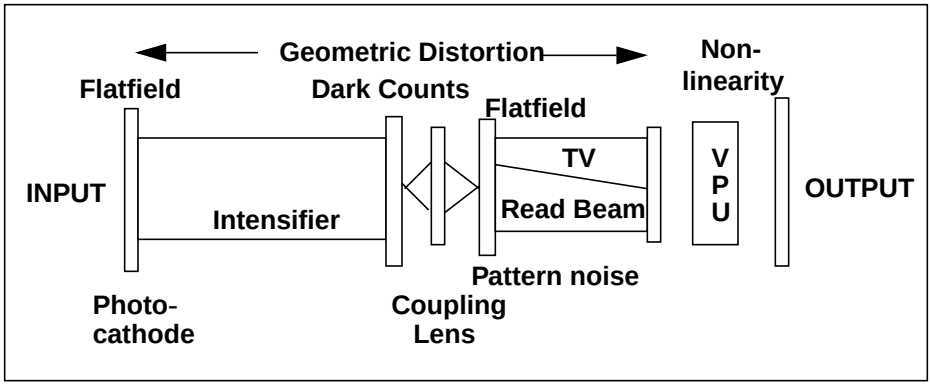

The ideal calibration algorithm applies to the raw data the inverse transformation to that which converted the input image to the output image. Each step would apply the corrections in reverse order, starting with the nonlinearity correction. In practice, the individual components of the ideal transformation are not known accurately, so such a process is unrealistic. Therefore, some of these effects are addressed only partially in the pipeline while others are not corrected at all. The following sections describe the limitations of these calibrations and their effects on the uncorrected image characteristics.

7.2 Nonlinearity

At high count rates, the video processing unit (VPU) of the FOC *undercounts* photon events, resulting in a nonlinear count rate. At even higher count rates, the detector saturates. An image whose counts have saturated will develop a dark hole, with a bright crescent appearing to one side (see Figure 4.6). The FOC remains linear to much higher count rates for point sources than for uniform

sources.[1] Table 7.2 gives the nonlinearity and saturation thresholds separately for extended and point sources and the different formats and modes of the FOC. Here, a uniform source is defined to be one in which the flux varies by less than +/– 10% on scales of 10 pixels, and the nonlinearity threshold is defined to be the count rate at which the FOC exhibits nonlinearity at the 10% level.

Table 7.2: Nonlinearity Parameters for Extended Sources and Point Sources

		Uniform Source		Point Source (for peak count rate)	
Camera	**Format**	**N (nonlinear)**	**N (saturation)**	**N (nonlinear)**	**N (saturation)**
f/96	512 zoom x 1024	0.04	0.11	0.15	0.45
	512 x 1024	0.08	0.37	0.5	1.5
	512 x 512	0.15	0.73	1.0	3.0
	256 x 256	0.60	2.93	4.0	12.0
	128 x 128	2.40	11.7	16.0	48.0
f/48	512 zoom x 1024	0.03	0.07	0.09	0.27
	512 x 1024	0.05	0.26	0.35	1.05
	512 x 512	0.06	0.52	0.70	2.10
	256 x 256	0.40	2.09	2.80	8.40
	128 x 128	2.40	8.40	11.3	33.9
f/48 SPEC	256 zoom x 1024	0.03	0.13	0.18	0.53
	256 x 1024	0.10	0.52	0.70	2.1

If the count rate from a point-like target is in the nonlinear regime, you should take special precautions when determining its brightness. For example, you might consider measuring the flux in the wings of the PSF and scaling them to a linearly exposed PSF. Unfortunately, no reliable and robust method exists for correcting nonlinearity in the FOC. There are, however, a couple of useful approaches for correcting some of the nonlinearity in calibrated FOC images, depending on whether the intensity distribution uniform or point-like.

Nonlinearity is introduced at the last stage of the FOC imaging process, so you should apply any nonlinearity corrections before geometrically correcting and flatfielding the image. The correction to apply to a given pixel depends on both the count rate in the pixel and the rates in neighboring pixels. If the count rate remains relatively constant over scales of 10–20 pixels or so, then the nonlinearity will be more severe than for a single pixel with the same count rate surrounded by pixels with a lower rate, such as in the center of a stellar PSF.

1. A typical photon event is several pixels by several pixels in size, and for extended (or *uniform*) sources the photon events at a given pixel affect those at the neighboring pixels.

This procedure was extended by Greenfield in *FOC ISR* 074. He hypothesized that the actual flux distribution within a given aperture was not as important as the mean count rate. By looking at pre-launch test FOC images he was able to determine that convolving images of PSFs with a circular aperture with radius 5.5 pixels yielded a nonlinearity correction very similar to what a flatfield would give. A more detailed discussion of this procedure is beyond the scope of this manual, but readers are referred to *FOC ISRs* 074 and 073 for some suggestions on how to deal with nonlinearity for stellar fields.

If the count rate for a *uniform* source is in the nonlinear regime, but below the saturation value, it is possible to correct the pixel values for nonlinearity using the **fflincorr** task in the STSDAS **foc.focphot** package. The **fflincorr** task uses the FOC linearity curve which has been derived for uniform sources from internal lamp flatfields. The linearity curve follows the formula $\rho = a(1 - e^{(-r/a)})$, where ρ is the observed count rate, *a* is the uniform source saturation count rate as given in Table 7.2, and *r* is the *true* count rate. This correction can be applied only for small or moderate nonlinearity; it is not valid for high nonlinearity. Users should beware that these methods are somewhat preliminary, and they are not guaranteed to correct (or even improve) all types of data. Do not apply this correction blindly.

7.3 Geometric Correction

The current geometric correction algorithm is good at correcting the gross characteristics of the FOC's geometric distortion, rectifying it to 0.5 pixels rms over most of the imaging format. However, the plate scales and orientations of FOC images are known to be time-dependent. The maximum change in scale from just after switch-on until the FOC has stabilized fully was measured during the initial orbital verification to be approximately 0.3%. A systematic study of the time dependence of the plate scale has not been done since, but repeated observations in the crowded-field analysis of fine-scale distortions (see page 6-6) did show plate scale differences of 0.1–0.2% even after the FOC had been warmed up for a long time. Angular rotations on the order of 0.1% from exposure to exposure can also occur. The pipeline does not attempt to correct for time-dependent aspects of the geometric distortion, and this deficiency can lead to astrometric errors between images taken at different times.

Geometrically corrected images displayed with high contrast close to the background, often show relatively low-frequency *fringes* with scale lengths of between 40 and 100 pixels (see Figure 4.5). This effect, a product of the geometric correction procedure caused by the algorithms used in re-binning the data, is merely a modulation of the noise characteristics of the data. The mean intensities in the image are not affected.

7.4 Flatfield Residuals

There are currently four UNI (flatfield) files for the *f*/96 camera at 1360, 4800, 5600, and 6600 Å and two UNI files for the *f*/48 camera at 3345 and 4800 Å. The UNI files have been derived from heavily smoothed flatfields. Thus, they do not flatten small-scale features, such as scratches and reseau marks, that exist in the flatfield response and can affect your photometric accuracy.

How much the small scale features affect the accuracy depends greatly on the type of data and the method of analysis. In some cases, careful treatment can improve the calibration. Figures 7.2 and 7.3 show relatively high signal-to-noise full-format flatfields obtained in the UV for the *f*/96 and *f*/48 cameras, respectively. Many of the features to be discussed here are evident in those figures.

7.4.1 Border Effects

The borders of FOC images suffer from corruptions arising both inside and outside the detectors. Among the most obvious external effects are the finger-like shadows cast by the occulting fingers (two occulting fingers for *f*/96 and the slit location finger for *f*/48.) In addition, square masks in front of both detectors shadow the upper left and lower left corners of the *f*/96 image (upper and lower left) as well as the lower right corner of the *f*/48 image. Furthermore, geometric correction transforms the straight edges of the original raw images into curved edges, most noticeable on the left and right sides.

Internal border effects show up in a few bad rows at the top and bottom of the raw image and the left-most columns of the raw image as well as a significant number of columns at the beginning of the scan line (right side of the image). In all FOC images, the internal border effects are present regardless of format; however, they do change from one format to another. In particular, the corrupted pixels at the beginning of the scan line arise from defects in the beginning of the sawtooth in the scanning waveform. The corrupted beginning is about 5% of the scan line for most *f*/96 formats In the *f*/48 detector it gets progressively worse for smaller formats (from about 5% for the full format to about 25% for the 128 x 128 format). The horizontal stripes seen in the bottom left of the *f*/96 image result from a ripple instability of the coil drivers at the beginning of a frame scan. None of these effects are normally correctable.

Figure 7.2: f/96 External UV Flatfield Image

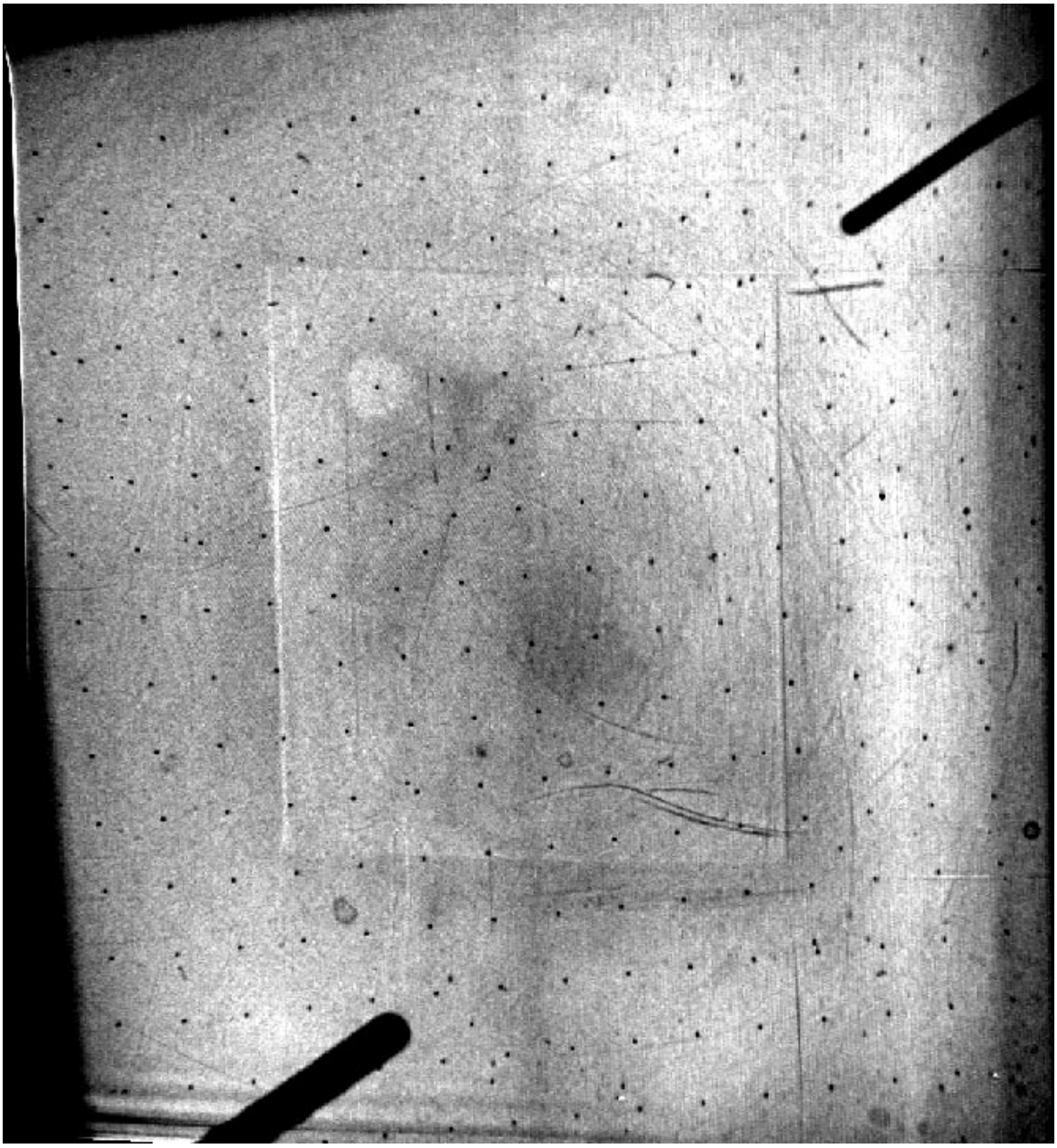

Figure 7.3: f/48 External UV Flatfield Image

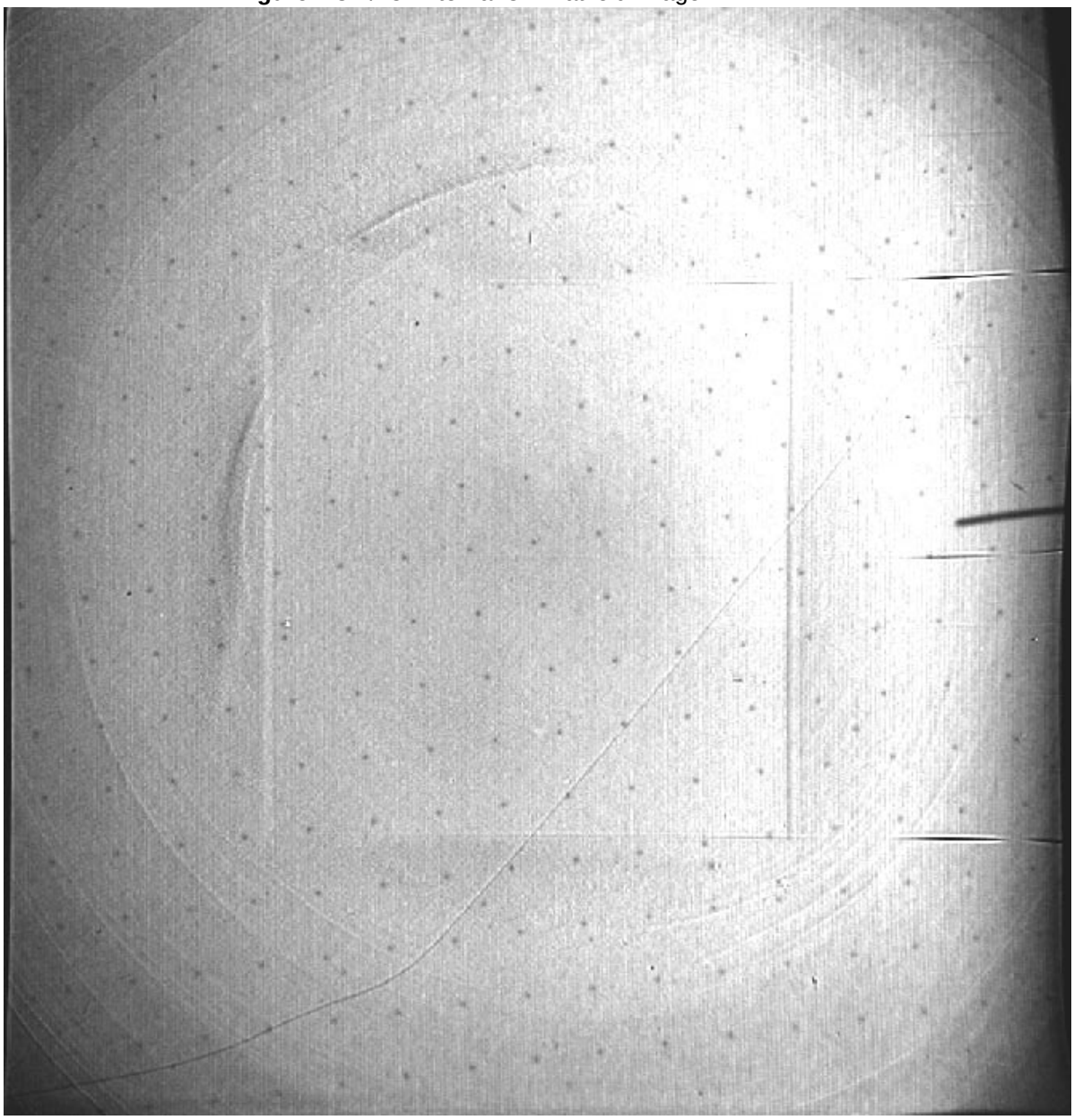

7.4.2 Video and Digitizing Defects

The narrow line running from the bottom left corner to the upper right corner (clearly visible for *f*/48, less so for *f*/96) is due to the read beam of the television camera not being completely blanked before it flies back to the beginning line at the end of a frame scan. This effect, along with a change in path, becomes more noticeable in smaller formats. The narrow horizontal features at the right edge, especially at lines 256, 512, and 768, are due to noise glitches on the scan coil driver caused by changes in the most significant bits of the line counter. The central 512 x 512 pixels in both cameras are outlined by sharp changes in

sensitivity. Heavy use of the 512 x 512 format has burned a charge discontinuity into the camera target array at the edges of this format. None of these effects is normally correctable and the affected areas should be treated as bad pixels.

7.4.3 Reseau Marks, Scratches, and Blemishes

A regular grid of reseau marks used to measure detector distortion spans both detectors' photocathodes. These reseau marks have about 90% opacity and are not normally worth trying to flatfield. In addition to the reseau marks, there are various scratches and blemishes, much more numerous in the *f*/96 camera. The scratches and blemishes generally appear much deeper in the far-UV—as much as 30% opacity for some scratches. Because the pipeline flatfield correction is heavily smoothed, none of these effects will be flatfielded out. Hence, photometry of sources which fall on or near these image defects can be compromised.

The **imedit** task in the **images** package or the **rremovex** task in **focphot** package can be used to repair such cosmetic defects in images having a source that falls on a reseau mark or small scale blemish. These tasks replace the values of the affected pixels with the average values of their neighboring pixels. Great care, however, must be taken in interpreting photometric results for sources which are directly affected by such image defects (i.e., in which the peak of the source falls on or immediately adjacent to an image defect).

7.4.4 Pattern Noise

Pattern noise, neither fixed nor constant in magnitude, constitutes another source of non-uniformity. Two types of patterns are often present, although not always easily seen in low count extended areas or flatfields. The more noticeable one is an approximately sinusoidal pattern with its peaks and troughs oriented at an approximately 45 degree angle and a period of 3.35 pixels for *f*/96 (it is just barely discernible in Figure 7.2). It is believed to originate from a moiré effect between a TV tube grid and the diode array on the target. The amplitude of the pattern depends on the count rate in the area. In flatfields with count rates between about 0.02 and 0.1 counts pixel^{-1} s^{-1} for a 512 x 512 format, the rms amplitude of the pattern is about 5% of the flatfield counts for *f*/96 and about 2.5% for *f*/48 (the peak deviations from a flat response due to this pattern are at least twice these values). At lower count rates, threshold unknown at this time, the pattern disappears. On the other hand, the pattern intensifies when count rates are in the nonlinear regime and thus is much more easily seen. In fact, it is a quick way of recognizing serious nonlinearity in an image.

A second pattern arises from some form of interference with an FOC digital timing waveform that has a four-pixel period. It shows up as vertically striped patterns on the flatfields (visible in Figure 7.2). Although very coherent in orientation and frequency (in the raw image), the details of the modulation do not appear to remain constant in either phase, waveshape, or amplitude from image to image. The rms amplitude of this pattern in moderate count-rate flatfields, is

approximately 2.5% for both cameras. Like the 45 degree pattern, this pattern seems to disappear at low count rates.

Given the nonlinear nature of the amplitude of these patterns and their variability in position (phase), there is no general method for correcting them. When count rates are moderate across most of the image, i.e., from an extended object or PSF halos, Fourier techniques can sometimes proves useful in removing the pattern. The main purpose of these techniques should be viewed as providing aesthetically pleasing images rather than as improving photometric accuracy.

7.4.5 Large Scale Variations

Large scale variations are those spatial variations having relatively low spatial frequencies, i.e., 20 or more pixels. The UNICORR step in the pipeline attempts to remove such variations from the image. Large scale variations in the response of the FOC do not appear to depend strongly on wavelength between 1300 and 6000 Å; generally speaking, the large scale response does not change more than 10% for all pixels except at the edges and corner of the full format. Beyond 6000 Å, the flatfields begin to change significantly, generally with poorer relative sensitivity towards the corners.

Obtaining flatfields in the UV requires a great deal of spacecraft time for each wavelength desired. At the moment, only one UV flatfield each exists for the *f*/96 and *f*/48 camera (at 1360 and 3727 Å respectively). It is not likely that there will be any more UV flatfields obtained for *f*/48.

The *f*/96 large scale response appears to be accurate to 1 to 2% rms over the most of the photocathode at the wavelength where it was obtained, excluding the edges and corners, and regions where the scanning oscillations are significant. The accuracy for *f*/48 is estimated to be 2 to 4% rms over comparable areas.

7.4.6 Time Variability

A small amount of temporal variability has been observed in the flatfield response; it is largest just after the FOC is turned on and begins taking exposures. Changes of about 1 to 2% are seen with respect to the flatfield response after an hour of exposures. The changes for *f*/48 are about twice as large. In general the response at turn on is higher at the center and weaker at the edges of the full format.

7.4.7 Format-Dependent Effects

The FOC flatfield depends on the video format used (Greenfield and Giaretta, 1987, *FOC ISR* 024). You cannot just divide an image by a flatfield derived from the corresponding subsection of the full-format field, even if you take great care to align the two images so that the reseau marks overlap. This effect was suspected to be due in part to the limited resolution of the geometric distortion field provided by the reseau marks and the resulting change in the apparent pixel size with

position. More detailed analysis by Greenfield using the new geometric correction method described on page 6-5 showed that these suspicions were ungrounded. The variations in sensitivity with position truly depend on the video format. At this time, however, the appropriate correction files have not been derived, although the possibility of applying a format-dependent flatfield does exist within the current FOC pipeline.

7.5 Format-Dependent Sensitivity

The sensitivity of the FOC depends on the format being used. The overall (OTA + COSTAR + FOC) central absolute quantum efficiency $Q(\lambda)$ in counts photon^{-1} (DQE), plotted in Figure 4.3 and tabulated as a function of wavelength in Table 11 of the *FOC Instrument Handbook* (version 7.0), refers to the 512 x 512 format. Because the DQE is a function of detector format whose cause is unknown (see *FOC ISR* 075), we give in Table 7.3 the sensitivities of the other formats, relative to the 512 x 512 format. Typical uncertainties in these numbers are approximately 5%.

Table 7.3: Format-Dependent Sensitivity Ratios

Camera	Format (FxL)	Relative Sensitivity
f/96	512*z* x 1024	1.25
	512z x 512	1.45
	512 x 512	1.00
	256x256	1.20
	128x128	1.23
f/48	512*z*x1024	1.44
	256*z*x1024	1.28
	512x1024	1.02
	512x512	1.00
	256x256	0.85

The pre-COSTAR overall (OTA + FOC) central absolute quantum efficiency Q(λ) in counts photon^{-1} (DQE) with no filters in the beam is plotted and tabulated as a function of wavelength in Figure 28 and Table 12 of the *FOC Instrument Handbook,* version 3.0, for the FOC imaging and spectrographic configurations. The data represent the product of in-orbit measurements for the *f*/96 camera and ground-based measurements of the *f*/48 absolute quantum efficiency, reflectance measurements of the OTA primary and secondary mirrors witness samples and an arbitrary dust covering factor of 10%. Pre-COSTAR data are not automatically corrected for format-dependent sensitivity effects.

7.6 Background

The FOC suffers from various types of background, the most important of which are thermal electrons, Cerenkov radiation from high energy particles, geocoronal emission lines, zodiacal light, and light scattered within HST from the bright Earth or Moon. Because the particle-induced background levels are essentially unpredictable, the FOC pipeline does not attempt to remove the background from a geometrically corrected and flatfielded image. In practice, most astronomical data analysis procedures derive the background locally as needed, so pipeline background removal is unnecessary.

The levels, spatial distribution, and time variation of the principal sources of background are discussed below to help you decide whether the background on your images might be astronomically interesting or is merely an instrumental effect. For a more thorough discussion, see the *FOC Instrument Handbook*.

7.6.1 Detector Background

The detector background arises primarily from thermal electrons at the first photocathode and high energy particles. The dark current due to thermal electrons is rather lower than the particle-induced background, at approximately 2×10^{-4} counts/sec/pixel. This background source is likely uniform over the field and temporally stable and does not show the reseau marks as dark holes. The particle-induced background is caused by high-energy electrons and protons which generate intense flashes of Cerenkov radiation as they pass through the photocathode window. The FOC's video processing unit (VPU) cannot distinguish the photons from these flashes from celestial photons, and so they appear as a background. The flux of these particles rises strongly over the South Atlantic Anomaly (SAA), but even well away from the SAA, they are the principal contributor to the background of most FOC images. For most of the useful orbit of HST, the particle-induced background is of the order of 7×10^{-4} counts sec^{-1} pixel^{-1} on the *f*/96 side, and $1\text{-}3 \times 10^{-3}$ on the *f*/48 channel. Upward fluctuations of these values are sometimes recorded. Because the particle-induced background generates photons, its spatial distribution looks like a flatfield, except

the shadows at the edges of the field caused by obstructions in the FOC beam between the aperture plate and the photocathode are not present. The reseau marks are between the photocathode faceplate where the Cerenkov radiation originates and the photocathode, so they will show up in exposures dominated by such backgrounds.

7.6.2 Geocoronal Emission Lines

The most important contributors to the background at ultraviolet wavelengths are geocoronal emission from Lyman-α (1216 Å) and the O I triplet at 1304 Å, which are relevant only during daytime observations. From on-orbit measurements using the *f*/96 camera, the former background has been found to vary with solar zenith distance (ZD); see Sections 6.4, 6.5, and 7.0 of the *FOC Instrument Handbook*, version 7.0, for more details. When the zenith angle is less than 160 degrees, the Lyman-α emission is zero.

For O I 1304, the background is less than 5×10^{-5} counts/sec/pixel for solar zenith distances (ZDs) of more than 90 degrees, rising nonlinearly to about 8×10^{-4} counts sec^{-1} $pixel^{-1}$ at ZD of 25 degrees.

For *f*/48, these numbers should be multiplied by a factor of about four, reflecting the pixel-size difference.

7.6.3 Zodiacal Light and Diffuse Galactic Background

The contributions to the FOC background from zodiacal light and diffuse galactic background have not been measured with the telescope in orbit, so you should assume that the information in the *FOC Instrument Handbook*, version 7.0, is the best available. Typically, the particle-induced background dominates in an *f*/96 image under all but the most extreme conditions (e.g., on the ecliptic and pointing as close to the sun as constraints allow), when the zodiacal background and detector background become comparable. Similarly, the diffuse galactic background can be ignored for almost all situations.

7.6.4 Scattered Stray Light

Normally, the FOC background is dominated by the detector, by zodiacal light in the visible, and by geocoronal Lyman-alpha and diffuse galactic light in the far UV. However, stray light reaching the OTA focal plane due to scattering from the baffle system, the OTA tube, and dust on the mirror can dominate the background when a bright object such as the sun, moon, or the bright Earth limb is nearby. In-orbit calibrations of this stray light have been performed by P. Bely and D. Elkins using a solar spectrum combined with the Earth's and the moon's albedo. Only for observations where the limb angle is less than 50 degrees from either the moon or the Earth will stray light have an illumination brighter than 23 V magnitudes per $arcsec^2$ at wavelengths greater than 3400 Å. More details on the

determination of the stray light contribution and its wavelength dependence can be found in Section 6.5 of the *FOC Instrument Handbook*, version 7.0.

7.7 Filter Induced Image Shifts

The FOC filter wheels hold the filters roughly parallel with the photocathode of the FOC, but slight offsets can shift the image position. The offset of the F320W filter, an image shift of 80 pixels, means a centered target is thrown about 80 pixels towards the edge of the image when the F320W filter is put in place.

Most FOC filters in the visible band induce an image shift of over 7 pixels, or over 0.1”, in an *f*/96 image. These effects can confuse the identification of an object imaged through different filters if the appropriate filter shifts are not taken into account. They can also make it difficult to obtain the proper offset for a dispersed prism image. Table 7.4 provides the observed filter shifts as seen in calibration data. The given offsets, good to +/- 1 pixel, are measured relative to the position an object would have through the F120M filter.

Table 7.4: Filter Induced Image Shifts Relative to F120M Image (good to +/- 1 pixel)

Filter	x Shift (pixels)	y Shift (pixels)
F120M	=0	=0
F130M	0	0
F140M	0	0
F140W	-1	2
F152M	0	0
F170M	0	0
F165W	1	1
F175W	-1	1
F190M	1	0
F210M	1	0
F220W	-1	2
F231M	1	-3
F253M	-1	3
F275W	-1	2
F278M	-2	4
F307M	-2	5
F320W	-73	46
F342W	-1	-2
F346M	-5	6
F372M	-4	6

Table 7.4: Filter Induced Image Shifts Relative to F120M Image (good to +/- 1 pixel) (Continued)

Filter	x Shift (pixels)	y Shift (pixels)
F410M	-12	17
F430W	1	8
F370LP	0	2
F480LP	-1	1
F486N	-6	16
F501N	11	0
F502M	-1	-7
F600M	24	11
F550M	-1	-5
F1ND	0	0
F2ND	1	0
F4ND	0	-1
F6ND	0	0

7.8 Errors in Absolute Photometry (f/96)

The absolute photometric accuracy of FOC observations depends on several factors. This section will not discuss those sources of error that arise from errors in the flatfield correction and associated effects (e.g., pattern noise). The remaining errors most likely arise from: 1) errors in the published fluxes or variations in fluxes of the spectrophotometric stars used to calibrate the absolute DQE, 2) errors in the assumed PSFs, 3) errors in the assumed filter transmission curves, 4) format dependence effects, 5) temporal variability in the FOC detectors, and 6) the spectrum of the source. This section will summarize the current understanding (or lack thereof) of these errors. As the *f*/48 detector is much more poorly calibrated, it will be discussed separately. For a summary of FOC accuracies, see Figure 8.4.

- ***Errors in the spectrophotometric standards.*** The spectrophotometric standards used for the FOC DQE determination are on the flux scale derived from correcting IUE spectra of the white dwarf G191B2B to conform to the pure hydrogen model of Finley (see Colina and Bohlin, *AJ* 108, 1931 (1994)). The spectra of the standards used here (BPM16274 and HZ4) were corrected using the same function. While it is difficult to assign a formal uncertainty to the predicted filtered fluxes due to errors in the spectrophotometry, assigning an error of +/– 3% is probably conservative enough.
- ***Errors in the assumptions for the PSF.*** Because the in-orbit calibrations relied on large aperture photometry, there should be very little sensitivity to details of the PSF or changes in the PSF. This source of error should con-

tribute less than 1% error to the derived efficiencies. (Note that quite the opposite is true when deriving total fluxes of stars from core-aperture or PSF-fitting photometry techniques).

- ***Errors in the assumed filter transmission curves.*** Although the filter transmission curves were carefully measured on the ground, that does not preclude some sort of subsequent degradation or change in performance. There has been no unambiguous evidence for changes in any particular filter's bandpass. There is some evidence that the redleaks of some filters differ significantly from their published values.
- ***Format dependence.*** A variation of sensitivity with video format has been noted. In particular, Table 7.3 shows the relative response of the more common *f*/96 formats with respect to the 512 x 512 imaging format. These determinations are not known completely accurately. Most of the absolute sensitivity calibration observations used the 256 x 256 format, so the uncertainty in the calibration of the format dependent sensitivity for this format enters into the uncertainty for all the formats. The uncertainty is approximately 3%. No such table has been derived for *f*/48. Note that if the image is calibrated using the PHOTFLAM from the image and the PHOTMODE keyword value indicates the format used, then no re-calculation of the absolute sensitivity is required.
- ***Variability of f/96 DQE.*** The overall throughput of the FOC has been monitored over the three years before the first servicing mission, and in the UV since the servicing mission. The only evidence for change has been an ~3% decline in the sensitivity over three years, independent of wavelength. From the time COSTAR was installed until mid-1996, there was no significant sensitivity change in the ultraviolet, but a slow downward trend of approximately 10% per year has been seen in the UV since then.
- ***Source spectrum.*** The value of PHOTFLAM averages F_λ over the bandpass. Situations where the detected flux distribution is skewed in wavelength can lead to large errors in assigning the absolute sensitivity calibration to the adopted (pivot) wavelength, especially when the wideband filters are being used or where redleak plays a significant part. If there is any doubt as to whether there are significant color effects, observers are advised to use **synphot** or **focsim** to check their absolute fluxes. FOCSIM is an FOC simulator that can be run under IRAF at STScI or from a WWW form found on the FOC world wide web pages. This error is very dependent on the filter being used and the source spectrum, so no rules of thumb about its magnitude can be given.

7.9 Absolute Sensitivity of the f/48 Detector

The DQE of the *f*/48 camera was never calibrated systematically because the existing spectrophotometric standards are generally too bright and the *f*/48 relay has no neutral density (ND) filters to attenuate their fluxes. A calibration program

was developed and run in December 1993, after COSTAR was installed but before it was deployed. The results of this program are presented in *FOC ISR* 077. This study indicated that the sensitivity from about 1800 Å to 3000 Å appears to be about 60% of the prelaunch estimate of sensitivity, with some uncertainty because the data used to derive this factor were less than ideal.

In general, *f*/48 fluxes must be considered quite uncertain. A typical error estimate of +/– 30% is appropriate.